Implantable polymer/metal thin film structures for the localized treatment of cancer by Joule heating

Kwabena Kan-Dapaah, Nima Rahbar, Christian Theriault, and Wole Soboyejo

Citation: Journal of Applied Physics **117**, 165301 (2015); doi: 10.1063/1.4918271
View online: https://doi.org/10.1063/1.4918271
View Table of Contents: http://aip.scitation.org/toc/jap/117/16
Published by the American Institute of Physics

JOURNAL OF APPLIED PHYSICS **117**, 165301 (2015)

Implantable polymer/metal thin film structures for the localized treatment of cancer by Joule heating

Kwabena Kan-Dapaah,[1,2] Nima Rahbar,[2,a)] Christian Theriault,[4] and Wole Soboyejo[1,4]
[1]*Department of Materials Science and Engineering, African University of Science and Technology, Abuja-FCT, Nigeria*
[2]*Department of Biomedical Engineering, University of Ghana, Accra, Ghana*
[3]*Department of Civil and Environmental Engineering, Worcester Polytechnic Institute, Worcester, Massachusetts 01609, USA*
[4]*Department of Mechanical and Aerospace Engineering, Princeton University, Princeton, New Jersey 08544, USA and Princeton Institute for Science and Technology of Materials (PRISM), Princeton University, Princeton, New Jersey 08544, USA*

(Received 3 March 2015; accepted 2 April 2015; published online 22 April 2015)

This paper presents an implantable polymer/metal alloy thin film structure for localized post-operative treatment of breast cancer. A combination of experiments and models is used to study the temperature changes due to Joule heating by patterned metallic thin films embedded in poly-dimethylsiloxane. The heat conduction within the device and the surrounding normal/cancerous breast tissue is modeled with three-dimensional finite element method (FEM). The FEM simulations are used to explore the potential effects of device geometry and Joule heating on the temperature distribution and lesion (thermal dose). The FEM model is validated using a gel model that mimics biological media. The predictions are also compared to prior results from *in vitro* studies and relevant *in vivo* studies in the literature. The implications of the results are discussed for the potential application of polymer/metal thin film structures in hyperthermic treatment of cancer. [http://dx.doi.org/10.1063/1.4918271]

I. INTRODUCTION

Treatment for early-stage breast cancer typically involves mastectomy (surgical removal of whole breast) or lumpectomy (breast conservation). Both procedures are normally followed by radiation therapy to remove any residual cancer cells. Although mastectomy has a low recurrence rate,[1] it is an aggressive form of treatment for early-stage breast cancer. Therefore, treatment modalities that could enhance the use of lumpectomy by eliminating residual breast cancer cells with limited side effects are needed. Clinical studies have shown localized hyperthermia to be an effective technique that can kill breast cancer cells safely in the intact breast with minimal damage to surrounding healthy cells.[2–7]

Interstitial magnetic hyperthermic treatment, which involves the implantation of biomaterials (thermoseeds) with magnetic properties, is one of the best developed localized hyperthermia techniques.[8–10] After implantation of the thermoseeds, heat is generated when an alternating magnetic field (AMF) is applied. The material properties of the thermoseeds determine the mechanism of heating. Metallic thermoseeds (normally nickel-based alloys) heat due to eddy currents.[11] However, different clinical *in vivo* studies have highlighted issues related to their biocompatibility.[10] These include issues such as corrosion and fibrous encapsulation.[12] Recently, magnetic nanoparticles-based thermoseeds have been shown to have the potential to overcome biocompatibility issues.[13–16] However, problems related to nanoparticle aggregation and instability[14–16] continue to hinder the transitions to clinical applications.

Our research group has previously reported *in vitro* hyperthermia *via* a direct voltage driven coil-based implant.[17] The implant consisted of metal thin film (heater) embedded in a biocompatible polymer, poly-dimethylsiloxane (PDMS), substrate. This has been shown to kill or reduce the viability of breast cancer cells in the vicinity of the elevated temperature fields that surround the device. The conditions for hyperthermia were achieved by applying a voltage of 1.5 V to the thin film using a battery. However, it is important to note here, that, for *in vivo* applications, wireless powering technology can be used in place of the battery as the power source.[18,19] This will ensure that the device is fully embedded in the tissue and controlled remotely. We have also reported *in vitro* simultaneous hyperthermia and drug release studies, using paclitaxol loaded thermo-responsive hydrogels of poly-n-(isopropylacrylamide) (PNIPA) incorporated within our hyperthermia implant.[20,21] About 90% of the loaded drug was released after 2 days of hyperthermia conditions.[21]

In order to move the above device to *in vivo* applications, estimation of the damage zones created by the device in biological media is essential to enable the assessment of its potential to kill post surgery residual cells. In this work, the *in vivo* thermal performance of our device during hyperthermia treatment of breast cancer following lumpectomy[23] procedures (see Fig. 1) is explored using a three dimensional coupled finite element method (FEM). The model includes: solutions to the Laplace's equation for electrical potential; predictions of the evolution of temperature using the bioheat

a)Author to whom correspondence should be addressed. Electronic mail: nrahbar@wpi.edu

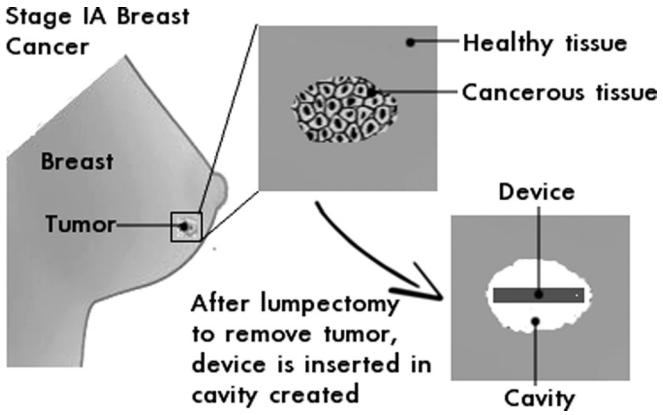

FIG. 1. Concept of treatment modality. Schematic of how a polymer/metal alloy thin film structure could be used for post-operative treatment of cancer.

equation; and calculations of the thermal damage/dose using cumulative equivalent minutes. Such models enable a realistic assessment of *in vivo* thermal performance of the device. The effects of blood perfusion (BP), device geometry, and treatment time on the temperature distribution and thermal dose were also explored. The implications of the results are then discussed for the potential application of polymer/metal thin film structures in hyperthermic treatment of cancer.

II. PROBLEM FORMULATION

In order to fully characterize and predict tissue damage caused by our Joule heating device, the spatial and temporal distribution of heat must be accurately determined. The device is inserted in the region of interest, such that its large surfaces are perpendicular to the growth axis of the tumor as shown in Fig. 1. The objective of the treatment is to maintain a uniform temperature (>42 °C) distribution in the targeted region.

A coupled electro-thermal FEM model is proposed for the prediction of thermal field distribution and the computation of thermal dose. The analysis was performed on three-dimensional domains for *in vitro* and *in vivo* scenarios.

A schematic of the FEM model is presented in Fig. 2. Note that, $\mathbf{\Omega}_1$ is the treated domain, $\mathbf{\Omega}_2$ is the polymer matrix domain, and $\mathbf{\Omega}_3$ is the electrically resistive layer (heater). Boundaries Γ_1, Γ_2, and Γ_3 correspond to the domains $\mathbf{\Omega}_1$, $\mathbf{\Omega}_2$, and $\mathbf{\Omega}_3$, respectively.

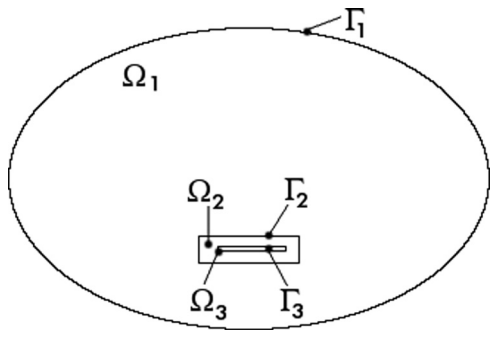

FIG. 2. FEM modeling. Schematic diagram of coupled thermo-magnetic set-up used for analysis.

A. Heat generation

Joule heating is caused when moving charges, accelerated by an applied voltage, collide with ions in the medium and give up some of their kinetic energy. Considering the resistive layer (thin film) as a conducting medium, we used the Laplace's steady-state equation [Eq. (1)] to compute the electrical potential distribution, V, in the coil. This gives

$$\nabla \cdot (\sigma \nabla \mathrm{V}) = 0, \tag{1}$$

where σ is the electrical conductivity of the material. The electric field and current through the resistive layer are related by Ohm's law given as

$$\mathrm{J} = \sigma \mathrm{E}, \tag{2}$$

where J is the current density and E is the electric field. The heat power per unit area, $\dot{q}_A$, produced inside the thin film is given by

$$\dot{q}_A = dQ_J, \tag{3a}$$

where

$$Q_J = J \cdot E \tag{3b}$$

Q_J is the power density and d represents the thickness of the resistive layer. Experimental studies have shown that the electrical behavior of conductive materials is temperature-dependent. However, their effects are insignificant within the operating temperature range used in our study (37 °C and 45 °C). A voltage difference was applied at the terminals of the coil, such that one end of the wire was set to an electrical ground and the other end was set to an electrical potential of V_{in}. All other boundaries were set as electric insulation/continuity. The coil represented a heat source and the heat was dissipated into the surrounding polymer matrix through its surface and then to the tissue.

For biological media, Pennes model[24] gives the effects of heat generation due to constant blood perfusion, Q_p, and metabolic heat, Q_m. Q_p is defined as

$$Q_p = \rho_b c_b \omega_b (T_b - T), \tag{4}$$

where ρ_b, ω_b, c_b, T, and T_b are the density, blood perfusion rate, specific heat capacity, temperature, and temperature of blood, respectively.

B. Heat transfer

The temperature distribution in solids due to an external heat source can be determined by the Fourier heat conduction equation. This is given by

$$\rho c_p \frac{\partial T}{\partial t} = \lambda(T)\nabla^2 T + Q_{gen}, \tag{5}$$

where ρ is the density, λ is the thermal conductivity, c_p is the specific heat capacity at constant pressure, and Q_{gen} is the heat generation term. At the boundary between the surface of the breast and the external environment, the heat

transfer can be modeled via a Robin boundary condition as: $\mathbf{n}\cdot(\lambda\nabla\ T) = h\ \cdot(T_{ext}\text{-}T)$, where the heat transfer coefficient $h = 3.5\ W\,m^{-2}\,K^{-1}$, $T_{ext} = 20\,^{\circ}C$. At the chest wall, a prescribed temperature, $T = 37\,^{\circ}C$. Continuity, $\mathbf{n}\cdot(\lambda_1\nabla\ T_1 - \lambda_2\nabla\ T_2) = 0$, was enforced on all the interior boundaries. Initial temperatures in all domains of the model were set to the normal body temperature of 37 °C.

C. Thermal dose

The assessment of the lesion predicted by our model was described using the method developed by Saparato *et al.*,[25] which expresses the thermal dose as a cumulative equivalent minutes of exposure at 43 °C (CEM_{43}). CEM_{43} is defined as

$$CEM_{43} = \int_0^{t_f} R^{[43-T(t)]}dt, \tag{6}$$

where t_f is the treatment duration and R has a value of 0.25, when the temperature as a function of time, T(t), is less than 43 °C or 0.5 otherwise. We considered tissue with a CEM_{43} value of 28 min to be thermally damaged.[26]

D. *In vivo* predictions

The geometry of the device and a schematic illustration of the breast phantom with an embedded hyperthermic device are presented in Fig. 3. The hyperthermic device consists of an electrically resistive layer (heater) that is embedded into a biocompatible polymer shell. The device, which has a design chosen so that the two large surfaces will be perpendicular to the growth axis, was used in *in vitro* experiments in our already published work.[20] As shown in Figure 3(a), the electrically resistive layer was modeled as a wounded thin layer (width 0.02 cm and thickness of 0.0127 cm) with spaces between turns, S. The device has a square shape with side length, H. The polymer shell was modeled as a square block with side length, P = 1 cm, and a thickness of 0.2 cm.

Fig. 3(b) shows the breast phantom geometry. This was assumed to consist of fatty tissue with long and short axes lengths of 12 cm and 5 cm, respectively. The device (blue) was assumed to be embedded in a cavity produced after the removal of tumor. The dimensions of the breast were chosen to represent a computational domain that was large enough to reduce the potential effects of the breast geometry on the heat conduction around the device.

The properties of the materials that were used in the simulations were obtained from the literature.[30,31] Due to the pronounced changes in BP and thermal conductivity of tissues, reported temperature-dependent values were used.[27] To account for the temperature dependence of BP, Eq. (4) was multiplied by a scaling factor (SF) according to Ref. 28, SF, for the breast tissue (SF_b) was expressed as

$$SF_b(T) = \begin{cases} 1 + \exp\left(-\dfrac{(T-45)^2}{12}\right) & \text{if } T \le 45\,^{\circ}C, \\ 2 & \text{if } T > 45\,^{\circ}C. \end{cases} \tag{7}$$

Also, the temperature dependent thermal conductivity was obtained from[29]

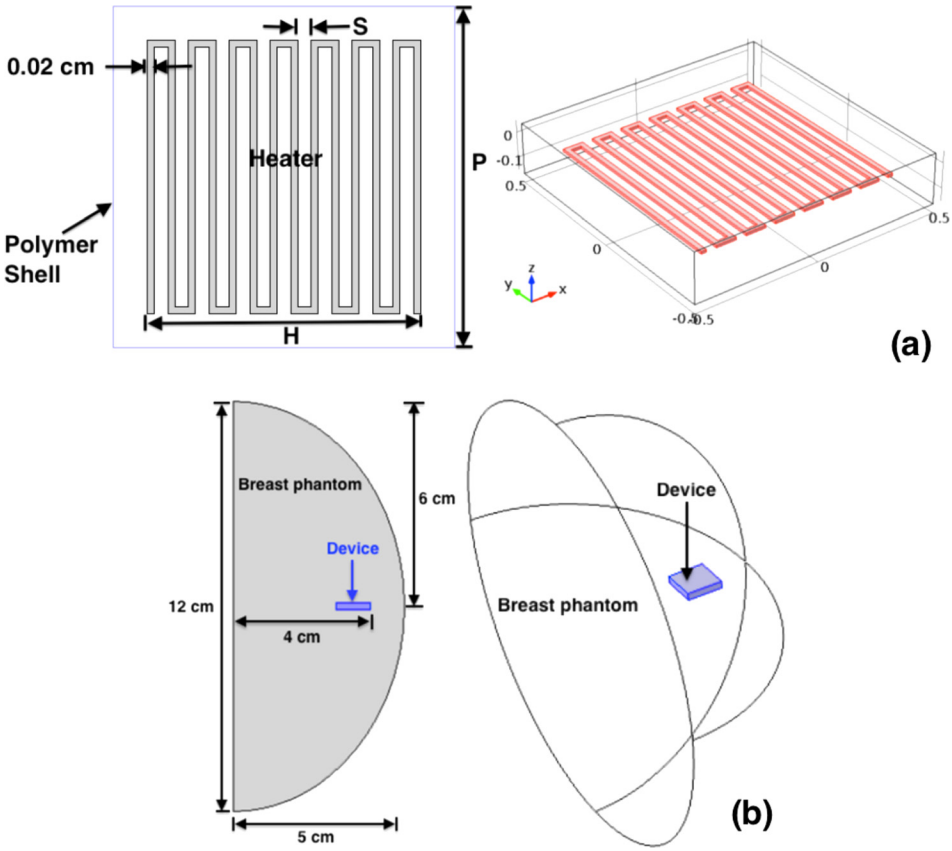

FIG. 3. The geometry used. (a) Schematics of the implantable biomedical device consisting of polymer matrix with an embedded electrically resistive layer (heater). (b) Schematics of breast phantom with the device (blue) embedded.

$$\lambda(\mathbf{T}) = 0.48[1 + 0.0028(\mathbf{T} - 293.15\mathrm{K})]. \quad (8)$$

The physical properties of the tissue, which were obtained from Bezerra *et al.*,[30] are summarized in Table I. The properties of PDMS were obtained from Ref. 31, while the properties of resistive layer materials were obtained from the COMSOL materials library.

Equations (7) and (8) were implemented as "analytical functions" in COMSOL, while materials properties were entered using the materials node.

E. Model implementation

The model was implemented using the COMSOL Multiphysics 4.3 a (Burlington, MA, USA) software package. The multiphysics "Joule heating" physics mode was used to simulate Eqs. (1)–(6). The numerical simulation was divided into the following 3 steps:

(i) the heat generation term was obtained from Eq. (3);
(ii) the temperature distribution was then determined as a function of time, using the volumetric power output from step (i) as the heat generation term in Eq. (5) and
(iii) the thermal dose was then calculated as a function of time, using the temperature history, and was used as the input to Eq. (6).

We used unstructured 3D tetrahedral mesh elements with minimum and maximum sizes of 0.01 cm and 1.2 cm, respectively. However, in the case of curved boundaries in the tissue model, curved mesh elements were used to improve the approximations. The mesh consisted of an average of 32 524 elements and 46 064 degrees of freedom. The numerical solutions were obtained using an iterative solution method, GMRES. This is a minimal residual algorithm based method that uses the Arnoldi process and incomplete LU factorization.[22] The simulations were performed on a mid-range workstation. The average computation time was less than 120 s.

F. Experimental validation

In an effort to validate the numerical model, we fabricated a device that consisted of a nichrome resistive layer that was embedded into a PDMS matrix (Fig. 4). It is important to note here that the nickel chromium alloy was simply a model material for the validation of the numerical model developed in this work and the device mimics the battery-powered structures that have been explored in our prior work.[17] Also, for the *in vivo* scenarios, other resistive heating elements such as gold and titanium alloys can be used to enhance the biocompatibility of the model system. In any case, the PDMS package was used to facilitate biocompatibility of the device during the *in vitro* experiments.

TABLE I. Physical properties of materials.

Material	λ [W m^{-1} K^{-1}]	ρ [kg m^{-3}]	c [kJ kg^{-1} K^{-1}]	ω [s^{-1}]	Q_m [W m^{-3}]
Breast[30]	0.48	1080	3000	0.00018	450
Blood[30]	…	1060	4200	…	…
PDMS[31]	0.15	970	1460	…	…

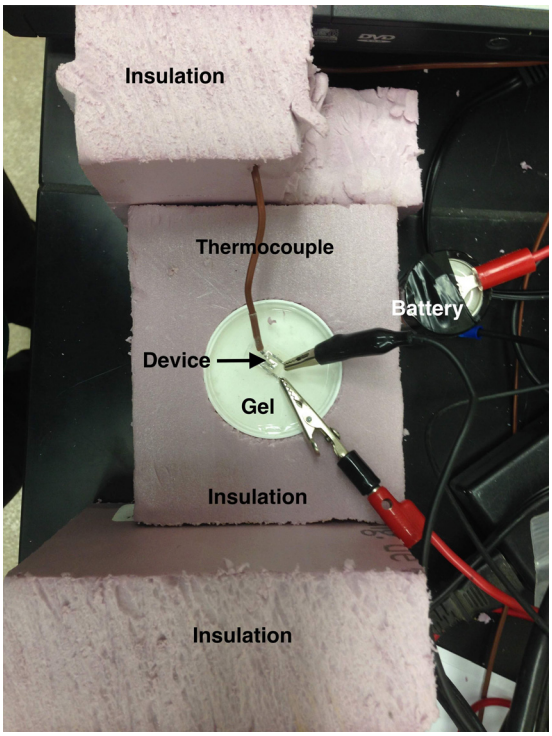

FIG. 4. Experimental setup. For the experiments, the following settings were used: time of application: 3 min, applied voltage: 1.5 V, polymer shell dimensions: 1 cm × 1 cm × 0.2 cm and heater dimensions: 0.7 cm × 0.7 cm × 0.0127 cm. Surrounding medium, that consisted of agar gel, was covered with insulated materials.

1. Materials

Commercially available nichrome sheet was obtained from H Cross Company, Moonachie, NJ, USA), while the PDMS Sylgard 184 silicone elastomer kit was purchased from Dow Corning Corporation, Auburn, MI, USA. These were used to prepare the nanocomposite samples.

2. Fabrication of Joule heating device

The device that was used for the experiments consisted of a 0.0127 cm thick electrically resistive nichrome layer that was embedded in a PDMS matrix with dimensions: 1 cm × 1 cm × 0.2 cm. A simple soft lithography technique was used to fabricate the PDMS matrix. First, the PDMS elastomer kit (base) and its curing agent were mixed together in a weight ratio of 10:1. This was then whisked vigorously with a spatula to produce a uniform mixture with adequate cross-linking. The resulting mixture was then placed in desiccator for about 60 min to ensure that the air bubbles were completely removed. Afterwards, the mixture was poured into molds containing the resistive layer and allowed to cure at 125 °C for 20 min.

3. Joule heating test

The fabricated Joule heating devices were placed in a container with a diameter of 5 cm and a height of 11.5 cm.

Thereafter, 3 ml agarose gel (1.2%) was added to the container. Voltage was then applied to the terminals for a duration of 3 min using MAX® D batteries (Energizer®, St. Louis, Missouri, USA). The actual voltage was monitored using a multimeter (Fluke 111, TEquipment.NET, Long Branch, NJ, USA). The evolution of the temperature at the surface was measured using thermocouples connected to signal conditioning connector block, SC 2345 (National Instrument Corporation, Austin, Texas, USA). The radial temperature spread was observed using an infra-red (IR) camera, ICI 7320 Scientific (Infrared Camera Inc., Beaumont, TX, USA).

III. RESULTS AND DISCUSSION

A. *In vivo* predictions

1. Temperature distribution and thermal dose coverage

Figs. 5(a) and 5(b) show the temperature distributions in and around the device. It is evident from the figures that the temperature distribution is non-uniform, favoring the central section of the electrically resistive layer, where the maximum temperature occurs. This maximum temperature has no direct effect on tissue, as it is reached on the surface of the thin copper layer, which is embedded within the polymer shell. Fig. 5(c) reveals that the shape of the resulted lesion (volume where 100% thermal dose is reached) is ellipsoidal and symmetric around the device.

The temporal evolution of temperature is presented in Fig. 6(a) for one of the large surfaces (indicated as I) and one of the surfaces on the side (indicated as II) of the device. For I, the model predicts an initial heating rate of approximately 0.19 °C/s, indicating that the temperature increase needed to achieve hyperthermia levels (~ 43 °C) within the tissue would take approximately 57 s. The model predicts much higher temperature at I than temperature at II, indicating that the orientation of the thin film and the size of the surface have an effect on the temperature levels achieved. This suggests the possibility of reaching hyperthermic temperatures at the interfaces between large surfaces and the tissue, while the interfaces between the edges and the tissue undergo slightly elevated temperatures. This result guides the placement of the device relative to the tumor growth axis. Furthermore, at both I and II, the temperatures approach a plateau after approximately 300 s. Fig. 6(b) predicts the axial (I) and radial (II) temperature spread away from the device. In both cases, the temperature decreases with increasing distance from the device. Also at given points, values for I were higher than those obtained for II.

Fig. 6(c) shows the axial temperature spread as a function of distance from the surface of the device. These are presented for different treatment times. The results show that, at given points away from the surface of the device, the temperature values increase with time. This is in agreement with results obtained from our prior studies.[17] It emphasizes the sensitive dependence of lesion created on time.

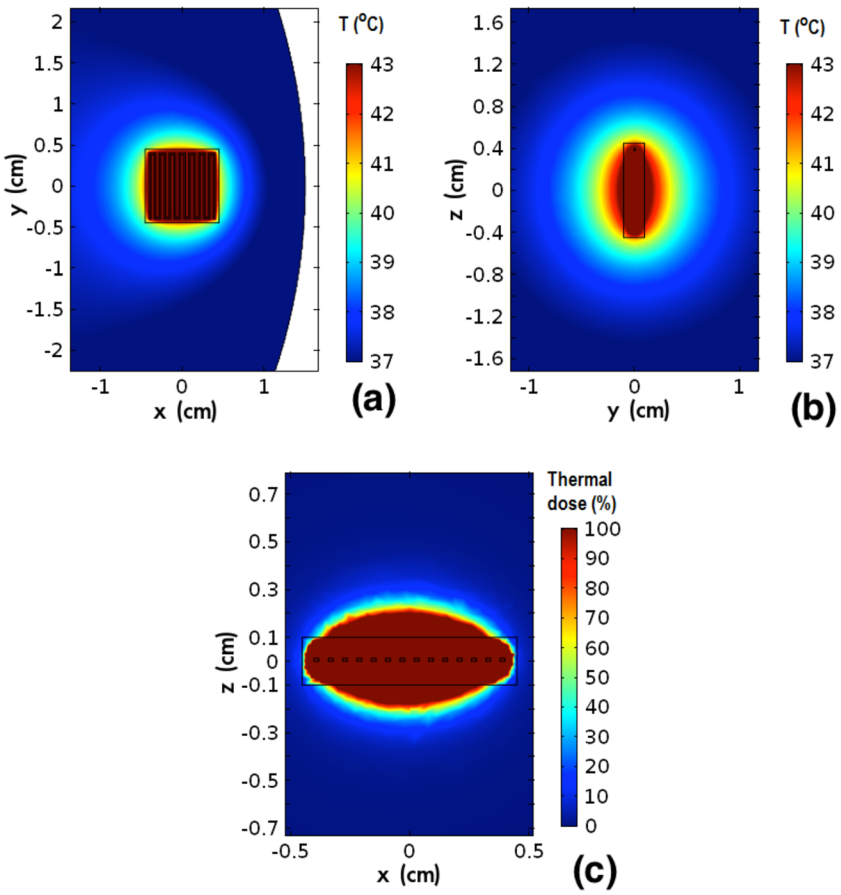

FIG. 5. Temperature profile results of FEM model. (a) Temperature distribution, xy plane. (b) Temperature distribution, yz plane. (c) Thermal dose coverage, xz plane around device (polymer shell: $1 \times 1 \times 0.2$ cm, thin layer: $0.8 \times 0.8 \times 12.7 \times 10^6$ cm and coil spacing: 0.04 cm) after a source voltage of 2 V is applied for 15 min.

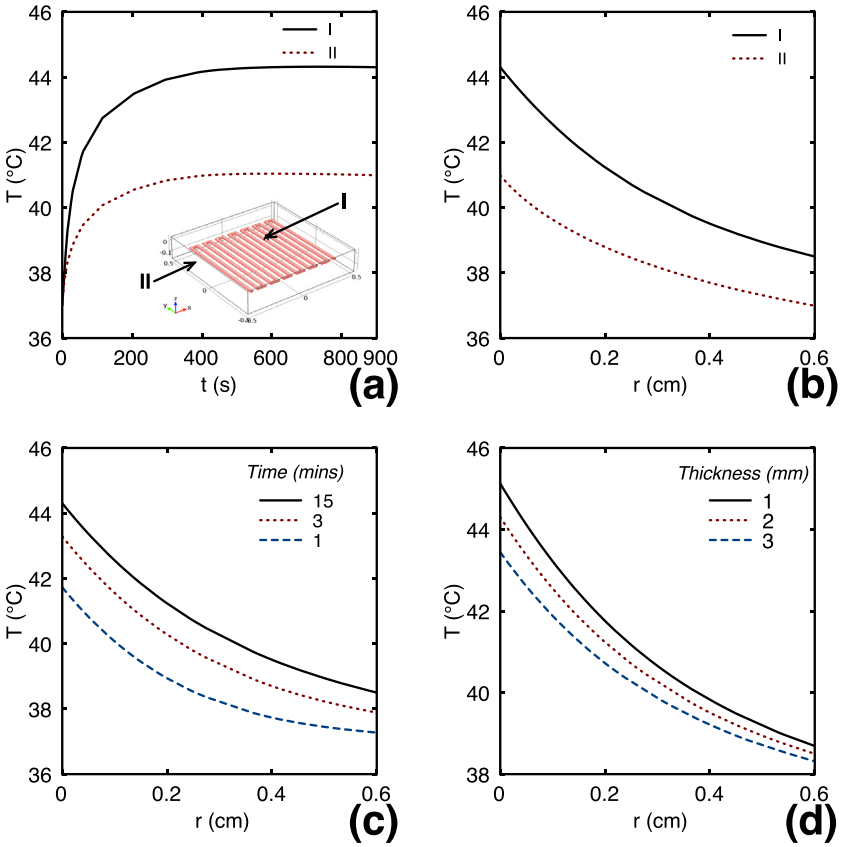

FIG. 6. Temperature as a function of time or distance. (a) Temperature as a function of time, (b) axial (I) and radial (II) temperature spread away from the surfaces of the device, and (c) axial and radial temperature spread away from the surface "I" for different thickness of the polymer shell after a voltage of 2 V is applied for 15 min.

2. Effects of geometry

Fig. 6(d) shows the axial temperature spread as a function of distance from the surface of the device for different thicknesses of the polymer shell. The temperatures increase with decreasing polymer shell thickness, for a given distance from the surface of the device. Hence, for instance, at a distance of 0.1 cm away from the surface "I" (see Fig. 6(a)) of the device, the predicted temperature value was ∼43.19 °C for a polymer shell thickness of 1 mm. This decreased, respectively, by ∼2% and ∼4%, when the thickness was increased to 2 mm and 3 mm.

B. Experimental validation

1. Validation of FEM model with experimental measurements

In the simulation model, blood perfusion [Eq. (4)] and metabolic heat terms were omitted, since they were not applicable to the model conditions that were examined. However, all other experimental conditions were implemented in the model. Fig. 7(a) shows the temporal dependence of the temperature on the surface of the gel. The experimental data and the numerical predictions are presented for the first 3 min of heating. The results show that the predictions are in good agreement with the experimental measurements.

Note that the error bars in Fig. 7(a) represent the error ranges in the experimental measurements, which were obtained for three runs at each individual time point. A maximum uncertainty of 1.2 °C was obtained from the experiments. Also, the predictions from our model diverged between 2% and 6% from the experimental results.

The deviations of the experimental data from numerical predictions can be attributed to the uncertainty in placement of the thermocouple, as well as fluctuations in the fluctuating DC voltage source. Fig. 7(b) shows the radial temperature distribution on the surface of the gel. It includes experimental data and numerical predictions for the first 3 min of heating. A maximum uncertainty of 1.1 °C was obtained. The predictions also diverge by 4% to about 7% from the values obtained from the experiments.

2. Comparison of model predictions with in vitro *and* in vivo *scenarios*

It is of interest to compare the model predictions with previously published results from *in vitro* and *in vivo* experiments.

In the case of *in vitro* experiments reported by our research group,[17] the breast cancer cell line MDA-MB-231 (ATCC, Manassas VA) was grown at 37 °C in a humidified environment with atmospheric CO_2 levels. The cells were seeded for 12 h prior to the first heat shock treatment with an initial confluence of ∼50%, resulting in a ∼70% confluence sample. Using our implantable device, the center of the sample was brought to 55 °C, while the outside edge remained below 41 °C. Propidium iodine (PI) assays were then used to determine the amount and location of cell death within a sample. Cell death was assumed to be a function of the local temperature, and thus a guide for the heat diffusion.

The results showed that necrotic cell death was prevalent in regions close to the surfaces of the device where the temperature was high (>45 °C). However, moving away from the surface of the device and as the temperature

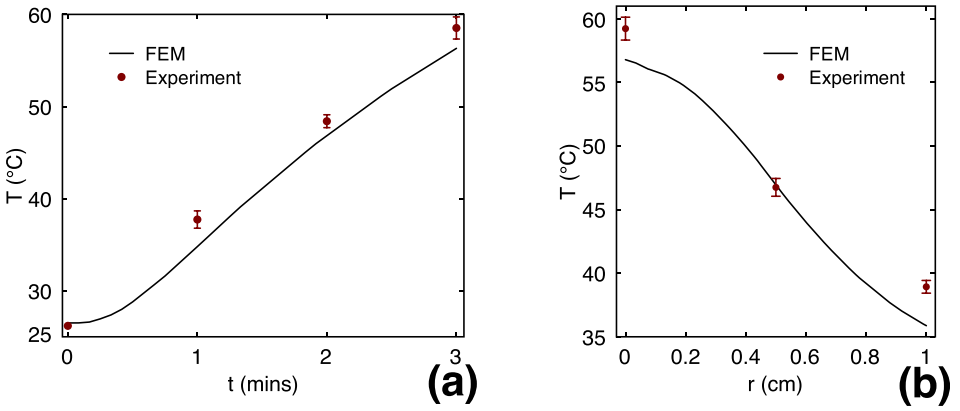

FIG. 7. Comparison of experiments and models. (a) The temporal dependence of the temperature and (b) radial temperature distribution on the surface of the gel after a voltage of ∼1.5 V is applied for 3 min.

decreased, the type of cell death was shown to be apoptotic. These trends are consistent with the predictions of temperature that was obtained from our predictions and described above (see Fig. 5). This suggests that the current model can predict the trends in cell death/tumor viability with increasing distance from the device surface. However, this requires some tuning in the CEM_{43} to obtain a good agreement between the measured and predicted results.

Similarly, in the case of *in vivo* conditions in which blood perfusion rates are important, our predictions show that depth of extension of tissue necrosis depends on factor such as device geometry and treatment time (see Sec. III A). These observations are consistent with experimental results obtained by Alvarado and co-workers.[32] They attempted to thermally kill residual malignant cells within 1 cm radius of the resected lumpectomy margin using a fluid-filled heated balloon with a radioactive source at its center. Glandular necrosis of breast tissue of Nubian-cross goats heated at 87 °C over selected time intervals of 1–24 min extended to a depth of 3.2–9.6 mm.

C. Implications

The implications of the current work are significant for the development of implantable hyperthermia devices that can be used for the treatment of breast cancer.

Our predictions suggest that the radial and axial temperature distribution in the vicinity of the tissue surrounding the tumor can be controlled in a way that could limit the killing of healthy cells. Furthermore, such devices can be modified and used in multimodal cancer therapy via simultaneous or sequential hyperthermia and chemotherapy, as shown in our prior studies.[17,21] The resulting devices[17] can be inserted into the cavity produced after lumpectomy. The inserted devices can be used as alternatives or used together with treatment modalities such as radiotherapy and chemotherapy. The device could then be removed after tumor recession or left there indefinitely without any potential harmful side effects due the biocompatibility of PDMS shell.

Although, *in vitro* experiments have shown promising results, the electrochemical power source makes the device too bulky for *in vivo* applications. However, light weight wireless powering can be used to replace the battery as the power source. Within this context, the battery is replaced by a receiver, attached to the implant, which harnesses energy provided by an external source.[33] Radio-frequency (RF) electromagnetic waves can then be used as an established means of energy transfer.[18] This could enable the device to be remotely controlled and recharged. Furthermore, using radio-frequency identification technology, temperature sensors can also be embedded in the device to provide remote and real-time monitoring of temperature and to enhance the efficacy of the treatment.[34,35]

Finally, our model remains a numerical model; thus, errors may appear from the considerations and simplifications made to realize it, such as assuming the thermal conductivity as a scalar value instead of a tensorial value. The tissue and blood are heterogeneous materials. Hence, the heterogeneity of these materials is the essential limitation of the model. The precision in evaluating the material properties used in the model can also play a key role in the accuracy of the results. Many theoretical studies have been carried out to calculate these properties.[29,36] However, the differences in the values presented by the different groups reflect the complexity of measuring these properties. The difficulty is intensified by the fact that real cells have a highly heterogeneous structure made of many constituents such as proteins and nucleic acids, as well as the inherent anisotropy in material properties such as thermal conductivities. This makes it difficult to implement them in numerical models such as the one developed for this study.

IV. CONCLUSION

In this work, a numerical finite element model was developed for the analysis of the thermal profiles in biological media subjected to heating by implantable Joule heating devices. The numerical predictions agree well with our *in vitro* results from prior studies, and relevant *in vivo* results reported in the literature. The study reveals that for given properties of the biological media, lesion characteristics (size and shape) can be controlled by factors such as device geometry, applied voltage, and treatment time. This suggests that our device has the potential to kill post surgery residual cells within reasonable radii away from the device surface.

ACKNOWLEDGMENTS

The authors are thankful for the financial support of the UG/Carnegie Foundation "Next Generation of Academics in Africa" Program, the World Bank STEP B Program, the

World Bank African Centers of Excellence Program, the African Development Bank, the Nelson Mandela Institution, and the African Capacity Building Foundation. Appreciation is also extended to Mr. Donald Pellegrino and Mr. Russ Lang (Worcester Polytechnic Institute) for technical support with the experiments.

[1]R. Katipamula, T. L. Hoskin, J. C. Boughey, A. C. Degnim, C. S. Grant, K. R. Brandt, C. L. Loprinzi, S. Pruthi, and M. P. Goetz, J. Clin. Oncol. **26**, 509 (2008).
[2]C. C. Vernon, J. W. Hand, S. B. Field, D. Machin, J. B. Whaley, J. van der Zee, W. L. J. van Putten, G. C. van Rhoon, J. D. P. van Dijk, D. G. Gonzalez, F. F. Liu, P. Goodman, and M. Sherar, Int. J. Rad. Oncol. Biol. Phys. **35**, 731 (1996).
[3]J. W. Hand, D. Machin, C. C. Vernon, and J. B. Whaley, Int. J. Hyperthermia **13**, 343 (1997).
[4]D. S. Kapp, Int. J. Rad. Oncol. Biol. Phys. **35**, 1117 (1996).
[5]R. W. Habash, R. Bansal, D. Krewski, and H. T. Alhafid, Crit. Rev. Biomed. Eng. **34**, 459 (2006).
[6]C. Alexiou, W. Arnold, R. J. Klein, F. G. Parak, P. Hulin, C. Bergemann, W. Erhardt, S. Wagenpfeil, and A. S. Lúbbe, Cancer Res. **60**, 6641 (2000).
[7]R. Jurgens, C. Seliger, and A. Hilpert, J. Phys.: Condens. Matter **18**, S2893 (2006).
[8]F. K. Storm, H. W. Baker, E. F. Scanlon, H. P. Plenk, P. M. Meadows, S. C. Cohen, C. E. Olson, J. W. Thonson, J. D. Khandekar, D. Roe, A. Nisse, and D. L. Morton, Cancer **55**, 2677 (1985).
[9]J. van der Zee, J. N. Peer-Valstar, P. J. M. Rietveld, L. de Graaf-Strukowska, and G. C. van Rhoon, Int. J. Radiat. Oncol. Biol. Phys. **40**, 1205 (1998).
[10]S. Krishnan, P. Diagaradjane, and S. Cho, Int. J. Hyperthermia. **26**, 775 (2010).
[11]I. A. Brezovich, W. J. Atkinson, and D. P. Chakraborty, Med. Phys. **11**, 145 (1984).
[12]I. A. Brezovich and R. F. Meredith, Radiol. Clin. North Am. **27**, 589 (1989).
[13]K. Kan-Dapaah, N. Rahbar, and W. Soboyejo, J. Appl. Phys. **116**, 233505 (2014).
[14]K. Kan-Dapaah, N. Rahbar, and W. Soboyejo, Med. Phys. **42**(5), 2203–2211 (2015).
[15]M. Kawashita, K. Kawamura, and Z. Li, Acta Biomater. **6**, 3187 (2010).
[16]S. Laurent, S. Dutz, U. O. Häfeli, and M. Mahmoudi, Adv. Colloid Interface Sci. **166**, 8 (2011).
[17]C. Theriault, E. Paetzell, R. Chandrasekar, C. Barkey, Y. Oni, and W. O. Soboyejo, Mater. Sci. Eng., C **32**, 2242 (2012).
[18]W. Phillips, B. Towe, and P. Larson, in *Proceedings of 25th IEEE Annual International Conference on Engineering in Medicine and Biology Society* (2003), Vol. 2, p. 1983.
[19]A. S. Y. Poon, S. O'Driscoll, and T. H. Meng, IEEE Trans. Antennas Propag. **58**, 1739 (2010).
[20]G. Fu and W. O. Soboyejo, Mater. Sci. Eng., C **31**, 1084 (2011).
[21]Y. Oni, C. Theriault, A. V. Hoek, and W. O. Soboyejo, Mater. Sci. Eng., C **31**, 67 (2011).
[22]S. Karaa, J. Zhang, and F. Yang, Math. Comput. Simul. **68**, 375 (2005).
[23]L. A. Newman and H. M. Kuerer, J. Clin. Oncol. **23**, 1685 (2005).
[24]H. H. Pennes, J. Appl. Physiol. **1**, 93 (1948).
[25]S. A. Sapareto and W. C. Dewey, Int. J. Radiat. Oncol. Biol. Phys. **10**, 787 (1984).
[26]P. S. Yarmolenko, E. J. Moon, C. Landon, A. Manzoor, D. W. Hochman, B. L. Viglianti, and M. W. Dewhirst, Int. J. Hyperthermia **27**, 320 (2011).
[27]S. Tungjitkusolmun, S. T. Staelin, D. Haemmerich, J. Z. Tsai, H. Cao, J. G. Webster, F. T. Lee, D. M. Mahvi, and V. R. Vorperian, IEEE Trans. Biomed. Eng. **49**, 3 (2002).
[28]T. Dřížd'al, P. Togni, L. Víšek, and J. Vrba, Radioengineering **19**, 281 (2010).
[29]F. A. Duck, *Physical Properties of Tissue: A Comprehensive Reference Book* (Academic Press, London, 1990).
[30]L. A. Bezerra, M. M. Oliveira, T. L. Rolim, A. Conci, F. G. S. Santos, P. R. M. Lyra, and R. C. F. Lima, Signal Process. **93**, 2851 (2013).
[31]D. Erickson, D. Sinton, and D. Li, Lab Chip **3**, 141 (2003).
[32]R. Alvarado, B. Mahon, C. Valadez, M. Caufield, S. Wadhwani, C. Hambleton, K. P. Siziopikou, A. T. Dickler, J. Gatta, and K. Dowlatshahi, Int. J. Hyperthermia **25**, 47 (2009).
[33]J. S. Ho, S. Kim, and A. S. Y. Poon, Proc. IEEE **101**, 1369 (2013).
[34]A. Vaz, A. Ubarretxena, I. Zalbide, D. Pardo, H. Solar, A. Garca-Alonso, and R. Berenguer, IEEE Trans. Circuits Syst. **57**, 95 (2010).
[35]K. Opasjumruskit, T. Thanthipwan, O. Sathusen, P. Sirinamarattan, P. Gadmanee, E. Pootarapan, N. Wongkomet, A. Thanachayanont, and M. Thamsirianunt, IEEE Pervasive Comput. **5**, 54 (2006).
[36]R. Pethig, *Dielectric and Electronic Properties of Biological Materials* (Wiley, New York, 1979).